

General Sky Models for Illuminating Terrains

Abstract

Sky models are quantitative representations of natural luminance of the sky under various atmospheric conditions. They have been used extensively in studies of architectural design for nearly a century, and more recently for rendering objects in the field of computer graphics. The objectives of this paper are to (a) describe sky models, (b) demonstrate how map designers can render terrain under various sky models in a typical geographic information system (GIS), (c) illustrate potential enhancements to terrain renderings using sky models, and (d) discuss how sky models, with their well-established standards from a different discipline, might contribute to a virtual geographic environment (VGE).

Current GIS hill-shading tools use a simple point light source to render terrain. General sky models allow the map designer to choose from a gamut of sky models standardized by the International Commission on Illumination (CIE). We present a computer application that allows the map designer to select a general sky model and to use existing GIS tools to illuminate any terrain under that model. The application determines the orientations and weights of many discrete point light sources that, in the aggregate, approximate the illumination provided by the chosen sky model. We discuss specific enhancements to terrains that are shaded and shadowed with these general sky models, including additional detail of secondary landforms with soft shadows and more realistic shading contrasts. We also argue that this process of creating hill-shaded visualizations of terrain with sky models shows parallels to other geo-simulations, and that basing such work on standards from the computer graphics industry shows potential for its use in VGE.

Keywords: Sky models, daylighting, hill-shading, shadowing, terrain illumination, VGE, CIE, geo-simulation.

1 Introduction

We make two propositions: (a) that a general sky model can represent almost all lighting effects currently used in terrain rendering, and (b) that virtual geographic environments (VGEs) concerned with three-dimensional visualization should support terrain rendering under arbitrary skies using state-of-the-art methods from the field of computer graphics. Examples of sky models are given and a rendering application is provided that allows map designers to illuminate a terrain under these models.

2 Sky Models

After a brief history of sky models, we describe the models currently used in GIS and computer graphics, and describe in more detail the commonly used “environment map” representation. In the following, “luminance” is the flux density of light emitted from a point in a direction. Luminance can come from the sky or from the ground. “Illumination” is a pattern of luminance from the sky.

2.1 Early Sky Models

Early systematic measurements of sky luminance were made in Chicago, Illinois and Washington, DC as reported by Kimball and Hand (1922), with results contributing to the best practices of the Illuminating Engineering Society (1993). Subsequent studies from throughout the world in the first half of the 1900s made important observations of daylight luminance (Gillette *et al.*, 1984). The first observation was that illumination has two logical end members associated with clear and overcast skies, with little variation seen in these two categories from place to place. The second observation was that, in the case of clear skies, illumination varied primarily with inclination of the sun above the horizontal. This is in line with a simple point source illumination model, which allows adjustment of azimuth and inclination of the illumination vector in hill-shading terrain, but does not account for the distribution of luminance in such clear skies.

Kimball and Hand (1922) suggested applications for their sky models, specifically the design of a type of roof to optimize daylight. Such “daylighting” studies continue to be used for architectural design considerations related to efficient use of energy for lighting, heating and cooling buildings (e.g. Hopkinson *et al.*, 1966; Robbins, 1985; Moore, 1985).

Kimball and Hand (1922) also noted that cloudy day skies had highest values of luminosity near their zenith, with decreasing luminosity toward the horizon. Twenty years later, Moon and Spencer (1942) formalized the luminance distribution for the **overcast sky model**. Luminance increases by a factor of three from horizon to zenith, with the distribution of

luminance showing radial symmetry with respect to the zenith. This went on to become an accepted standard for luminance distribution of the sky by the International Commission on Illumination (CIE) in 1955 (Nakamura *et al.*, 1985).

A **clear sky model** requires a more complex derivation, due in part to its lack of symmetry with respect to the zenith (assuming the sun on a clear day is not located directly overhead). The general construct for most such sky models begins with a “sky dome” (e.g. Nishita and Nakamae, 1974), where the sky is approximated as a hemisphere of very large radius centered over the object to be illuminated. Using this model, any distribution of illumination that can be mapped to a hemisphere can then be used to illuminate an object. In this construct, a point on the hemisphere has an azimuth and inclination from horizontal that corresponds to a direction from which the light is arriving.

Kittler (1967) was the first to come up with a rigorous derivation of the clear day sky model. A clear sky standard of luminance distribution was first adopted by the CIE in 1973 (Nakamura *et al.*, 1985). Derivations of sky models based on clear and overcast days eventually were incorporated into standards by the International Organization for Standards (ISO) as well as the CIE (ISO/CIE, 1996).

The **point source model** uses Lambert’s Law of Cosines to establish a simple relationship between the incident angle of illumination and the brightness of the surface unit. Additionally, if the surface behaves as an ideal diffuse reflector, issues of reflections among surface elements can be ignored with less loss in accuracy. This simplified model served as the de facto practice for hill-shading before computer-assisted cartography (Imhof, 1982), and continues as such to the present day (Kimerling *et al.*, 2011).

The **uniform illumination model** assumes a “sky dome” with equal brightness in all sectors. Although this uniform sky standard was not established by the CIE until 1970, uniform illumination was commonly used in daylighting calculations before the overcast sky model was adopted (Nakamura *et al.*, 1985). Uniform and overcast skies both result in renderings that lack directional shadowing effects.

Nakamura *et al.* (1985) gathered photometric measures of the sky over Japan using fish-eye lenses. They determined that actual sky conditions did not match clear or overcast standards, and developed their own intermediate sky model. Perraudau (1988) proposed three intermediate sky models: the intermediate overcast sky, the intermediate sky, and the intermediate clear sky. Perez *et al.* (1993) derived an “all-weather sky” model, and devised a method for incorporating common irradiance measurements to locally refine existing sky models. Their model’s framework includes a mathematical expression that is a generalization of the CIE clear sky formula. The formula includes five coefficients that can be adjusted to represent a gamut of potential skies, including an overcast sky.

Numerous sky models continued to be developed. Based on statistical methods applied to measures of sky luminance in Tokyo, Japan, Igawa *et al.* (1997) identified twenty patterns of luminance distribution. Kittler *et al.* (1998) used data from Tokyo, Japan, from Berkeley, California, and from Sydney, Australia to define fifteen sky types of relative luminance

distribution. Five were then assigned to the classes of overcast, clear, and transitional. With the preponderance of sky models, it became apparent that a general model was needed with parameters that could be modified to account for any sky model at any locality.

Such a model was proposed by Darula and Kittler (2002), and adopted as the **CIE general sky model** in 2004. Their model uses five different parameters and includes a table listing fifteen standard relative luminance distributions. Two parameters (a and b) define the relative gradation of luminance moving from the zenith toward the horizon with six standard gradation curves numbered I – VI. In addition, three parameters (c, d, and e) are used to define a scattering indicatrix. These parameters relate the relative luminance of each sector of the sky to its angular difference from the illumination direction, with these six standard indicatrix curves numbered 1 - 6.

2.2 Sky Models in GIS and Computer Graphics

Near the same time at the CIE general sky model was adopted, computer graphics research tackled more advanced sky models that included multiple atmospheric effects. One frequently used example is the work of Preetham *et al.* (1999), which approximated full spectrum daylight and atmospheric conditions used to render terrain models. The Preetham *et al.* model was adapted from the luminance-only model of Perez *et al.* (1993) to include two color channels. Renderings with the Preetham *et al.* model can show the terrain rendered at various times of day, and with variable “turbidity” due to haze. Although such effects are impressive on images showing both terrain and sky, the effect would be much less noticeable on the typical hill-shaded maps of terrain created by many map designers.

Recent computer graphics research continues in a similar vein. Sloup (2002) summarized atmospheric effects modeled at that time and introduced a numerical solution to the light transfer equation. Haber *et al.* (2005) numerically simulated radiation transfer in the atmosphere in order to better render twilight phenomena. Zotti *et al.* (2007) compared values from Preetham *et al.* (1999) to ISO/CIE (2004) CIE general sky luminance distributions and their own sky observations, and described ranges of turbidity for which the calculations break down. They suggested Haber *et al.* (2005) as a more rigorous approach.

2.3 Representation of Sky Models with Environment Maps

In a computer program, a sky model can be represented as a procedure that returns the radiance, $L(\theta, \phi)$, from a given direction.

Alternatively, a sky model can be represented as an environment map, a two-dimensional discrete sampling of the radiance function that can be stored in a table or in a graphics texture. Environment maps were originally used to store an image of the surrounding environment and to reflect that environment off of specular surfaces, making the surfaces

appear more realistic.

The original environment maps were called sphere maps (Miller and Hoffman 1984) and recorded the incident illumination in a table indexed by azimuth and elevation. Cube maps (Greene 1986) instead projected the environment onto a cube and stored each face of the cube in a texture for easier filtering and lookup. The dual paraboloid mapping (Heidrich and Seidel 1998) provided a better parameterization of the incident directions, which resulted in good-quality sampling in all viewing directions. Cube maps and the dual-paraboloid mapping are now implemented in graphics hardware.

3 Terrain Rendering Methods

Terrain in cartographic displays is often rendered using hill-shading tools provided with GIS software. These algorithms commonly calculate the brightness of a surface element using the angle between the surface normal vector and an illumination vector in the direction of the sun. But more information can be conveyed in the rendered terrain by using multiple light sources, or by determining how much of the sky dome is visible from each surface element, or by using a general sky model. Algorithms from computer graphics can now render a terrain at interactive rates under a dynamically changing sky model, while also incorporating interreflections among terrain elements (e.g. Sloan *et al.* 2002).

3.1 Point source illumination

An early mathematical approach to shading terrain was offered by Wiechel (1878). He derived a trigonometric formula using the aspect directions and angles complementary to inclination of the surface normal and illumination vectors to calculate an intensity for each surface based on Lambert's Law of Cosines. Such a methodology, however, would be difficult to implement on a smoothly varying topographic surface without first approximating it by a series of facets. Map designers instead often used the quantitative contour framework in concert with a direction of illumination to interpret more artistic and qualitative tones of gray for hill-shading (Yoeli, 1959; Imhof, 1982).

Yoeli (1965; 1966; 1967) led computer-based analytic visualization of terrain from a computational standpoint, despite shortcomings of effective computer display and output devices at the time (see discussion in Kennelly, 2002). Brassel *et al.* (1974) approximated hill-shading with special character sets on a line printer, and plotting continuous shades of gray was fully computer-automated by Peucker *et al.* (1974) using a digital elevation model (DEM) as the basis for analysis and visualization. Brassel (1974) extended such research by accounting for atmospheric variations with elevation.

The sky model used in today's GIS software is typically that of a point light source repre-

senting the sun. We assume this model is so prevalent in cartographic rendering because it is relatively easy to implement. It also results in a hill-shading effect that allows most map users to perceive the shape of the terrain (Kimerling et al., 2010, Slocum *et al.*, 2008, Robinson *et al.*, 1995).

3.2 Multiple-Point illumination

Imhof (1982) discussed techniques of using multiple illumination directions to better represent valleys or other landforms not apparent from the preferred illumination direction. In general, such techniques involve locally adjusting the direction of illumination. This approach is tailored to local landform geometries, and is in contrast to a single sky model that is applied to all terrain features.

One cartographic technique that explicitly defines the distribution (and color) of lights in the sky was suggested by Hobbs (1999) for his map of the Hawaiian islands. He used three illumination sources of various colors situated at 120 increments of azimuth. The resulting map is interesting, but the conceptual framework is more similar to Warn's (1983) idea of studio lighting than to that of a realistic sky model.

GIS research in insolation often uses multiple point illumination sources. One example of such an application is the Solar Analyst extension in ArcGIS (Fu and Rich, 1999; Fu and Rich, 2002). The intent of that application, however, is to estimate insolation values based on the location of the sun in the sky on multiple dates. It is not designed to use sky models to provide more advanced rendering of terrain.

3.3 Horizon-Based Illumination

Several approaches have sought to determine what part of the sky is visible from each point on the terrain, and to shade the point based on the fraction of the sky that is visible. These approaches necessarily compute the horizon as seen from each point on the terrain, since the horizon defines the boundary of the visible sky, and varies from point to point.

Iqbal (1983) described the "unit sphere method" in which a point is shaded in proportion to the area of visible sky projected onto a horizontal plane. Dubayah and Rich (1995) similarly described the "sky view factor" as the ratio of diffuse sky irradiance at a point to the total possible (unobstructed) irradiance on a flat surface. For isotropic skies, this can be computed from average zenithal angle of the surrounding horizon.

Determining the horizon at a point is very computationally expensive, as it can require inspection of every other point on the terrain, and this process must be repeated for every point. Several methods subsample the horizon at a point, p , by traversing the terrain in a number of fixed directions around p and finding the point of maximum inclination with re-

spect to p in each of those directions (Dozier et al 1981, Cabral *et al.* 1987, Max 1988, Wang *et al.* 2000). Interestingly, Max (1988) achieves soft shadows on the terrain by determining the fraction of the sun’s disk that lies above the horizon. These methods take computation time of $\mathcal{O}(n^{1.5})$ on average in a terrain of n points. Stewart (1998) provided a more efficient method that computes the sampled horizon at every point in time $\mathcal{O}(n \log^2 n)$. More involved methods (e.g. Heidrich *et al.* 2000) also compute interreflections on the terrain surface.

Ambient occlusion, also known as accessibility mapping (e.g. Miller 1994, Zhukov *et al.* 1998, Spitz and Requicha 2000, Iones *et al.* 2003), is an approach which computes, for each point of the surface, the solid angle of directions in which the outside environment is locally visible. This solid angle gives an approximation of the amount of light arriving at the point from the outside environment and permits shadowing from extended light sources to be estimated, much like the sky view factor of Dubayah and Rich (1995).

3.4 Full-Sky Illumination

The goal of rendering a terrain under full-sky illumination is to evaluate the rendering equation (Kajiya 1986) to determine the radiance, L , emitted at every terrain point, x :

$$L(x, \omega_o) = L_e(x, \omega_o) + \int_{\Omega} L(x, \omega_i) f(x, \omega_i, \omega_o) (N(x) \cdot \omega_i) d\omega_i , \quad (1)$$

where: L_e is the “self emitted” radiance; Ω is the hemisphere of directions centered on the surface normal, $N(x)$; ω_i is the unit vector in the direction *from which* incoming light is arriving; ω_o is the unit vector in the direction *toward which* outgoing light is leaving; and f is the bidirectional reflectance distribution function (BRDF) describing the ratio of the outgoing radiance to the incoming flux density.

Since the sky is assumed to be very distant from the terrain, there is no positional dependence on the sky radiance and $L(x, \omega_i)$ is often abbreviated as $L(\omega_i)$ for directions, ω_i , in which the sky is visible from x .

Monte Carlo methods (Halton 1970, Cook *et al.* 1984) are considered the “gold standard” way to evaluate the rendering equation and consist of tracing rays of light through the scene across multiple bounces with the terrain surface. Many variants of ray tracing exist that accelerate the computation at the expense of accuracy, but ray tracing is typically quite computationally expensive.

Classical radiosity (Goral *et al.* 1984) assumes an ideal Lambertian surface with constant BRDF (i.e. $f(x, \omega_i, \omega_o) = \frac{\rho}{\pi}$ for surface albedo ρ) and iteratively evaluates light transfer between surface patches of the terrain. Radiosity also produces very good renderings, but is again quite computationally expensive. But Keller (1997) described a fast method to exploit the graphics hardware with a set of virtual light sources to evaluate the radiosity solution.

3.5 Pre-computed Illumination

A sky model, $L(\omega)$, can be approximated as a sum of basis functions,

$$L(\omega) = \sum_i \alpha_i L_i(\omega),$$

where the L_i are the basis functions and the α_i are the weights of the basis functions. Each L_i basis function is itself a sky model. If the L_i are chosen well then a particular sky model, L , can be represented as a linear combination of the L_i . Advantages of this formulation are that a particular sky model can be compactly represented with a sequence of coefficients, α_i , and that a terrain can be rendered under any such sky model as a sum of pre-rendered terrains. The number of coefficients is typically small (under 100).

Sky models that are represented as a sum of basis functions permit very fast *interactive* evaluation of the rendering equation. In a precomputation step, the rendering equation is evaluated once for each of the basis functions individually. Let $T_i(x)$ be the radiosity of point x of the terrain rendered under the L_i sky model. Then, to render under a particular sky model, $L(\omega) = \sum_i \alpha_i L_i(\omega)$, we can simply compute a weighted sum of the already-rendered terrains:

$$T(x) = \sum_i \alpha_i T_i(x) \tag{2}$$

This is a very fast process and allows the sky model to be varied at interactive rates on the computer screen.

Nimeroff *et al.* (1994) used polynomials in the cosine of the angle between the sun and surface normal for their basis functions. These were chosen so that the sky model was “steerable”: any rotational transformation of the model could be represented with some linear combination of the basis functions. Nimeroff *et al.* demonstrated that clear skies, cloudy skies, and linear combinations of these skies could be modelled with their basis functions. Self-shadowing and surface interreflections could not be handled because the sky model described only the direct, unobstructed irradiance. Dobashi *et al.* (1995) used spherical harmonics as basis functions in their lighting models. Ramamoorthi and Hanrahan (2001) showed that only nine coefficients were necessary to determine irradiance to within 1% using spherical harmonics.

Sloan *et al.* (2002) showed that self-shadowing and surface interreflections could be pre-computed and modelled using the same spherical harmonics as were used to model the sky. This “precomputed radiance transfer” determined, for each surface point, a vector (for diffuse surfaces) or a matrix (for specular surfaces) that could be multiplied by the vector of sky model coefficients to determine the radiance of the surface point. Sloan *et al.* found that only nine to 25 coefficients were needed to accurately represent radiance transfer.

4 An Application for Rendering with General Skies in the GIS

Rendering of a terrain under a changing sky at interactive rates is a solved problem in computer graphics, but current GIS software does not even support rendering under static general skies.

To show the effects of general sky models and rendering with these models in GIS, we describe a method (and provide a corresponding software application in Section 4.4) to render terrains under general sky models *within the constraints of current GIS software*, with the hope that such standards from the field of computer graphics will be utilized in future VGEs.

4.1 Examples of Sky Models

This section describes five sky models that are available in the software application: the uniform sky, the overcast sky, the clear sky, the sharp sky, and the turbid sky. Each is described in terms of the sky radiance, $L(\theta, \phi)$, in all directions. Let

- (θ, ϕ) be the direction from which radiance arrives, with inclination θ equal to zero at the zenith,
- $(\theta_{sun}, \phi_{sun})$ be the direction of the sun, and
- γ be the angle between $(\theta_{sun}, \phi_{sun})$ and (θ, ϕ) .

In what follows, the sky radiance can be arbitrarily scaled to represent brighter or darker skies. In our application, the scaling of the sky radiance has no effect since, after the terrain illumination is computed from the sky radiance, we scale and bias the terrain illumination to lie within a range that is convenient to represent on the computer, typically 0...255 (8 bits) or 0...65535 (16 bits).

The **uniform sky** (Figure 1a) has the same radiance in all directions:

$$L(\theta, \phi) = 1$$

The **overcast sky** (Figure 1b) has a uniform component plus another component that increases toward the zenith. This was originally described by Moon and Spencer (1942):

$$L(\theta, \phi) = 0.33 + 0.67 \sin \theta$$

The **CIE general sky**, described by Darula and Kittler (2002), has five parameters to define various skies:

$$L(\theta, \phi) = (1 + c (\exp(d\gamma) - \exp(\pi d/2)) + e \cos^2 \gamma) (1 + a \exp(b/\cos \theta)) \quad (3)$$

Their exposition includes a normalizing term to ensure that the radiance is equal to one at the zenith. We do not include the normalizing term because it is redundant in our case, since we scale and bias the terrain illumination values to a fixed range. The variables a , b , c , d , and e are given various values to model different skies, as described by Darula and Kittler (2002).

The **clear sky** (Figure 1c) is brightest in the direction of the sun but diminishes in brightness less quickly toward the horizon than it does in other directions away from the sun. This sky is one case of the CIE general sky, described as “Type 11: White-blue sky with distinct solar corona”. In Equation 3, the parameters of the Type 11 sky are $a = -1$, $b = -0.55$, $c = 10$, $d = -3$, and $e = 0.45$. Note that this is *not* the “Type 12: CIE standard clear sky, low illuminance turbidity”, which has more illumination near the horizon than the Type 11 sky.

The **sharp sky** (Figure 1d) is bright in the direction of the sun and tapers off very quickly away from the sun. A constant term, a , is added for ambient illumination in all directions. The specularity increases with the s parameter:

$$L(\theta, \phi) = \begin{cases} \cos^s \gamma + a & \text{if } \cos \gamma > 0 \\ a & \text{otherwise} \end{cases}$$

The parameters of this sky can be chosen to approximate the classic point source rendering used in cartography. In the particular example of Figure 1d (and in the later Figures 6 – 8), the parameters of the sharp distribution are $a = 0.1$ and $s = 250$.

The **turbid sky** (Figure 1e) has less illumination from above and more illumination from the horizon than the clear sky. This is one case of the CIE general sky, described as “Type 14: Cloudless turbid sky with broad solar corona”. In Equation 3, the parameters of the Type 14 sky are $a = -1$, $b = -0.15$, $c = 16$, $d = -3$, and $e = 0.3$.

4.2 Terrain Illumination under a Given Sky Model

We will assume a perfectly diffuse terrain surface and will ignore surface interreflections. The radiance, $L(x)$, leaving a terrain point, x , due solely to reflected sky illumination is (Kajiya 1986)

$$L(x) = \frac{\rho(x)}{\pi} \int_0^{2\pi} \int_0^{\frac{\pi}{2}} V(x, \theta, \phi) L(\theta, \phi) \cos \gamma \sin \theta \, d\theta \, d\phi \quad (4)$$

where

- $V(\theta, \phi)$ is the “visibility term” which is 1 if the sky is visible from x in direction (θ, ϕ) and 0 if the sky is blocked from x in that direction;
- γ is the angle between the surface normal at x and the direction (θ, ϕ) and $\cos \gamma$ is the usual Lambertian hill-shading term ($\cos \gamma$ is clamped to the range $[0,1]$ for the purposes of hill-shading);
- $\rho(x)$ is the terrain albedo at x ; and
- $\sin \theta d\theta d\phi$ is an infinitesimal solid angle (measured in steradians) in the direction (θ, ϕ) , where inclination angle θ is zero at the zenith.

Radiance can be converted to luminance (which is the perceived intensity) using the CIE standard photopic luminosity function (Gibson and Tyndall 1923).

To render under a general sky *within the constraints of current GIS software*, we must cast the general-sky lighting problem as a point-lighting problem. We use the method described in Section 3.5 to render a terrain as a weighted sum of other rendered terrains (Equation 2) but require that each other terrain be rendered using point lighting in the GIS software.

Choosing a set of point light sources to approximate the continuous illumination of the sky dome is a Monte Carlo sampling problem. The integral of Equation 4 is estimated by N point sources in different directions, (θ_i, ϕ_i) :

$$L(x) \approx \frac{\rho(x)}{\pi} \sum_{i=1}^N V(x, \theta_i, \phi_i) L(\theta_i, \phi_i) \cos \gamma_i w_i \quad (5)$$

where w_i is the weight of the sample in direction (θ_i, ϕ_i) and is equal to the solid angle of the sky that this sample represents. Note that w_i corresponds, in the integral of Equation 4, to the infinitesimal solid angle, $\sin \theta d\theta d\phi$, of the sky centered around direction (θ, ϕ) .

To compute Equation 5 at all points of a terrain, the GIS is used to render a shaded and shadowed grid, G_i , for each direction, (θ_i, ϕ_i) . For G_i , the radiance of the point light source given to the GIS is $L(\theta_i, \phi_i)$ as defined by the chosen sky model. The GIS handles the visibility term, $V(x, \theta_i, \phi_i)$, through its shadowing computation and handles the Lambertian term, $\cos \gamma_i$, through its shading calculation.

The N shaded and shadowed grids are summed to produce a grid illuminated by the chosen sky model:

$$G(x) = G_\rho(x) \sum_{i=1}^N w_i G_i(x) \quad (6)$$

where $G_\rho(x)$ is a grid in which point x has value $\frac{\rho(x)}{\pi}$.

4.3 Computing Sample Directions and Weights

Given a sky model with a continuous radiance distribution, $L(\theta, \phi)$, two questions arise: How should the sample directions, (θ_i, ϕ_i) , be distributed and what should be their weights, w_i ?

Two strategies used in Monte Carlo integration are “importance sampling” and “stratified sampling”. Both strategies reduce the variance of the estimate of the integral, producing a result that is more likely to be accurate and that requires fewer samples.

Importance sampling places more samples where the integrand is larger; in the case of sky sampling, more samples are placed where the sky is brighter. Stratified sampling breaks the domain into strata, in each of which the variance of the integrand is expected to be small.

We use a slight modification of the method of Agarwal *et al.* (2003) to generate sample directions using both importance sampling and stratified sampling:

1. We start with a large number (typically about 10,000) of sky directions, chosen to have uniform spacing in inclination and azimuth. See Figure 2.
2. The sky radiance in each direction is computed from the chosen sky model. The standard deviation, σ , of these radiances is computed. The maximum radiance, L_{max} , is determined.
3. The directions are divided into n strata, s_1, s_2, \dots, s_n , with n chosen as the number of standard deviations between the minimum and maximum radiances. Stratum s_j contains directions with radiances between $(L_{max} - (j - 1) \sigma)$ and $(L_{max} - j \sigma)$. See Figure 3.
4. Each stratum, s_j , is allocated an approximately equal number of sample directions. (This is in contrast to the method of Agarwal *et al.* (2003) and is done to reduce perceptible artefacts¹ in exchange for some increased computational cost.) Samples are thus allocated according to importance, with samples being allocated more densely to areas of higher radiance, which are typically much smaller than areas of lower radiance.
5. Within each stratum, s_j , the sample directions are chosen with the algorithm of Hochbaum and Shmoys (1985): The first sample direction is picked randomly from among all of the directions within the stratum. Each subsequent sample direction in the stratum is chosen as the direction with the largest angular distance from all of the

¹The Agarwal *et al.* method allocates samples to strata in proportion to the importance measure (radiance times solid angle to the 0.25 power). We found that dimmer areas of the sky got very few samples with this method and the few, isolated samples tended to cast light like dim point sources, resulting in sometimes-perceptible sharp shadow edges. By allocating an equal number of samples per stratum, we push more samples into the dimly-lit regions, so samples in those regions become closer to each other and responsible for smaller solid angles, reducing the artifacts.

already-chosen sample directions. This results in good coverage of each stratum and in evenly separated sample directions within each stratum (Agarwal *et al.* 2003). See Figure 4.

6. The N sample directions are transformed to a set of N points on the unit hemisphere and the Voronoi diagram on the sphere is computed (Na *et al.* 2002). The weight, w_i , of the i^{th} sample direction is calculated as the solid angle subtended by the Voronoi cell of the i^{th} point. See Figure 5.

The result is a set of N sample directions, each having a weight equal to the solid angle of the sky that the sample direction represents. As seen in Figure 5, the algorithm concentrates many samples in those directions with bright light, but gives those samples low weight. The algorithm has a much less dense sampling in directions of low radiance and gives those samples more weight, in proportion to the larger solid angle that each sample represents.

Each of these directions, (θ_i, ϕ_i) , radiances, $L(\theta_i, \phi_i)$, and weights, w_i , can be used in the GIS to compute a shaded and shadowed terrain under the given sky model, using Equation 6 as described above.

Alternative methods could be used to generate sample directions. Kollig and Keller (2003) also use a Voronoi-based subdivision. Debevec (2005) uses a recursive rectangular subdivision which works well when there are many small, bright sources of light that are captured by small rectangles of the subdivision. However, for the smoothly varying skies that we want to model, the rectangular subdivision (adapted to the hemisphere) would probably yield a more variable estimator than one based on a Voronoi partition.

4.4 A Computer Application to Compute Directions and Weights

We developed a computer application that allows the map designer to choose a sky model and adjust parameters, including the azimuth and inclination, and the number of sample points used. The application shows sample terrains under the chosen illumination, allowing the map designer to immediately see the effects of different sky models and different parameter settings. Once the model and its parameters have been chosen, the application applies the algorithm described above to produce sample directions and weights. The application exports a comma-delimited text file containing values of azimuth, inclination, and weight (based on radiance). Instructions on utilizing the exported text file in the GIS with a Python script are provided with the application, which can be downloaded from <http://watkins.cs.queensu.ca/~jstewart/skyModels.zip>.

The sky models incorporated in the application include sharp, uniform, and Moon and Spencer's (1942) overcast sky. It also includes all 15 of Darula and Kittler's (2002) standard relative luminance distributions discussed in Section 2.2. We render terrain in Section 5 with two of these: a clear sky (General Type 12: CIE standard clear sky, low illuminance turbidity); and a turbid sky (General Type 14: cloudless turbid sky with broad solar corona).

5 Results and Implementation

Results of using this application, rendered with a vertical exaggeration of five times ($5\times$) and a Python script for shading and shadowing in ArcGIS are illustrated for the Valley and Ridge province of Pennsylvania, Mt. Hood in Oregon, and a portion of the Grand Canyon, Arizona. All DEMs were downloaded from <http://viewer.nationalmap.gov/viewer> (the National Map Viewer). The Valley and Ridge (632×628 cells) and Mt. Hood (764×942 cells) grids both are one arc-second (approximately 27×27 meter) data. The Grand Canyon ($1,486 \times 1,600$ cells) grid is $1/3$ arc-second (approximately 9 meter) data.

Figures 6 – 8 are rendered with six different illumination models (a – f). The first rendering (a) uses a traditional point source illumination, using an azimuth of 315° and an inclination of 45° . The three following maps have a directional component: sharp (b), clear (c), and turbid (d). The final two renderings have no variations in brightness with respect to aspect: overcast (e) and uniform (f). We refer to these as “non-directional” renderings because their sky illumination models exhibit no brightness variations with respect to azimuth.

We use 250 sky points for rendering these terrains. Kennelly and Stewart (2006) looked at the number of points necessary to render an urban DEM without artifacts. They demonstrated that 250 sky point sources are sufficient for detailed shading. Although terrain rendered in this study is generally smoother, sharp edges along ridges or cliffs can result in the same artifacts without sufficient sky points. All sky models use the default values for ambient light and specularity shown in Figure 1, except the “Sharp” model. Increased ambient light and decreased specularity make sharp illumination easier to distinguish from a point source illumination.

5.1 Valley and Ridge, Pennsylvania

The Valley and Ridge province (Figure 6) includes plunging folds of resistant layers of sedimentary rocks that create a sinuous pattern of sharp ridges. The axes of the plunging folds create broad ridges and valleys that tend to narrow from southwest to northeast.

The point source illumination rendering (a) clearly differentiates sloping terrain of various orientations. Areas facing northwest are uniformly bright, while those facing southeast are dark, a strong directional bias associated with the perceptual relief effect. Ridgelines and valleys are represented by sharp transition moving from northwest to southeast of bright to dark and dark to bright shading, respectively. The rendering could be described as having a shiny or glossy sheen.

With directional renderings in (b), (c), and (d) dark areas are not as dark and bright areas are not as bright. This reduces the directional bias while preserving the perceptual relief effect, and helps to distinguish more secondary features on the areas sloping to the southeast and northwest, respectively. Ridges have an increasingly brighter band towards the ridgeline

and valleys have a darker band near the edges of river channels. The gentle northwest facing slopes are most brightly illuminated with the turbid sky, as this sky has the greatest concentration of brightness closest to the horizon. These renderings lack a glossy sheen and suggest a style akin to rendering by pencil shading.

Non-directional renderings in (e) and (f) are similar to slope shading, as discussed by Imhof (1982). This rendering does not represent “the steeper, the darker” but, rather, “the less visible sky, the darker.” It is not possible to distinguish areas with northwest versus southeast aspect based on brightness. Ridgelines appear bright with darker shading on either side. This is apparent in the sinuous ridgeline and the broader noses of the two plunging anticlines. Stream channels appear as relatively bright, curvilinear features with edges of the channels shaded darker.

5.2 Mt. Hood, Oregon

Mt. Hood (Figure 7) is a stratovolcano in the Cascade mountain range with a summit elevation of 3,429 meters and a prominence of more than 2,300 meters. Mt. Hood has one prominent peak, with less conspicuous ridgelines (arêtes) and U-shaped glacial valleys along its flank.

While the point source illumination model (a) renders the northeast, northwest, and southwest flanks of the volcano brightly, the southeast flank appears dark. This results in the valleys and ridgelines being difficult to discern on this side.

The directional renderings in (b), (c), and (d) add brightness and detail to the southeast flank, making arêtes and glacial valleys more apparent. Overall patterns of brightness and darkness for such features are similar to appearance as those described for directional shading of the Valley and Ridge.

The non-directional renderings in (e) and (f) highlight local terrain, but may make identifying the overall volcanic landform more challenging. Although directional bias is mitigated, the perceptual relief effect is lost. Without cues from directional lighting, the map user may need to employ a strategy such as tracing ridge and valley lines to their nexus to identify the peak of Mt. Hood. We would not recommend using non-directional illumination for illuminating isolated peaks due to the loss of the three-dimensionality of the resulting map.

While ridgelines appear as bright traces, many valleys do not have the previously described pattern of a central brighter channel flanked by darker channel. This is likely due to the rivers in this area flowing in larger glacial valleys, and the relatively small variations in elevation associated with channel edges when compared to the overall relief of the landscape.

5.3 The Grand Canyon, Arizona

The Grand Canyon in Figure 8 is a negative relief feature carved approximately 1,800 meters into the Kaibab Plateau by the Colorado River. Layers of sedimentary rocks, with varying resistance to erosion, result in canyon walls with more and less steeply sloping sides. More sky light tends to be blocked moving deeper into the canyon.

The point source rendering (a) highlights sloping canyon walls, with shading variations apparent at ridgelines and at the canyon's bottom. The broad flat area representing the Colorado River and its narrow floodplain is clearly displayed as a ribbon of medium gray, but the tributaries flowing into the Colorado from the side canyons are not apparent.

The directional renderings in (b), (c) and (d) show contrasts between southeast and northwest slopes less starkly, revealing additional detail on these canyon walls. This variation from point source rendering is least apparent with the turbid sky, as much of the illumination coming from near the horizon does not penetrate far into the canyon. The Colorado River shows numerous subtle variations in shades of gray based on how much of the sky model's brightness is visible from a point on the river. Also, tributaries to the Colorado River can now be discerned at the bottom of side canyons.

The non-directional renderings in (e) and (f) show more symmetrical shading with respect to ridges and valleys. Although these maps seem to have hypsometric grayscale tinting darkening in deeper areas of the canyon, this is not the case. The canyon is shaded relative to the amount of the sky dome that is visible at any particular grid cell, and the distribution of brightness in the sky model. The centerlines of the Colorado River and its tributaries, depths from which a slightly greater amount of the sky would be visible, are more apparent and continuous as lighter, curving lines.

This is consistent with results from uniform sky models applied to urban elevation models in Houston, Texas (Kennelly and Stewart, 2006). Streets were darkest at the edge of buildings and became progressively brighter moving toward street centerlines. Street intersections also were brightest at their midpoint, much as the Colorado River becomes brighter at points where tributaries join the river.

6 Discussion

Rendering terrain with the use of sky models creates a geo-visualization using geo-simulation. In this sense, such methodologies could make important contributions to virtual geographic environments (VGE) as described by Lin *et al.* (2013). In a VGE workspace, the user can, among other things, conduct computer-aided geographic experiments (CAGEs) that correspond to the real world and its physical dimensions.

Geo-visualization is concerned with computation, cognition, and graphic design (Butten-

field and Mackaness, 1991), and virtual environments can empower such efforts (MacEachren *et al.*, 1999). Terrain representations including hill-shading have been classified under the cartographic field of “Analytical Cartography.” This more “analytical, conceptual and mathematical approach” to terrain representation (Moellering, 2000, p. 205) has been applied to both mathematical representations of the terrain (e.g. contours, triangulated irregular networks) and visualizations of the modeled terrain. The latter falls under the field of “Analytical Visualization,” as discussed by Moellering (2000, 2012).

Terrain representation studies provide a fairly simple, intuitive construct for visualizing geospatial data in three dimensions. Evidence of this status includes chapters on terrain representation (and analysis) in numerous introductory textbooks on geo-visualization, GIS, and cartography (e.g. Slocum *et al.*, 2008; Chang, 2011; Robinson *et al.*, 1995). Such a construct is often extended to 3D visualization of spatial information in general (e.g. Wood *et al.*, 2005; Moellering, 2012). Additionally, the landscape metaphor as defined by Fabrikant *et al.* (2010) offers some potential for expanding geographic thinking more generally into the realm of information visualization.

Geo-simulations tend toward human geography and its spatial interactions (e.g. Benneson and Torrens, 2004; Albrecht, 2005) and environmental simulations (e.g. Steyaert and Goodchild, 1994; Yuan, 1999). Regarding terrain, early algorithms designed for extracting drainage networks (O’Callaghan and Mark, 1984) were then incorporated into hydrologic models (Maidment, 1993) and then into something more closely resembling a VGE. Steyaert and Goodchild (1994) stress the importance of the move from what Maidment (1993) describes as a lumped-model to a distributed parameter approach. In the former, the spatial properties in the watershed are averaged without consideration of local effects; in the latter the spatial characteristics of detailed digital terrain and ancillary data are considered. By analogy, our sky modeling approach attempts to use a distributed sky model to refine the current lumped-model of a point illumination source representing all of the sky for terrain representation.

Another type of geo-simulation in terrain studies from which analogies might be drawn is visibility analysis. Given one location within a terrain grid, such analysis defines a viewshed or isovist based on which grid cells are visible from that location. Visibility graphs (O’Sullivan and Turner, 2001; Turner *et al.*, 2001) extend this concept by recording all visibility relations in the landscape. O’Sullivan and Turner (2001) note that visibility graphs require significant pre-processing, equivalent to calculating a viewshed for each cell in a DEM. Turner *et al.* (2001) apply these graphs to architectural settings, with uses including wayfinding and use of space.

Using sky models to shade terrain uses visibility analysis in a different manner. The technique can be conceptualized as defining what portion of the sky hemisphere is visible from each grid cell in the DEM (Section 3.3), and then summarizing all of the visible sky’s luminance and orientation with respect to the surface element, after which the grid cell is displayed in a shade of gray. Much as explanations of visibility analysis are also illustrated with lines of sight, numerous vectors of illumination can be thought of as beginning at the

sky hemisphere and ending at a small terrain element located at the center of the hemisphere. Shading would depend on sums of luminance, with cells of the DEM not visible along a particular vector having a shadow to represent that particular lack of intervisibility.

Although more computationally intensive than typical hill-shading using one illumination vector, this method could make a greater contribution to and provide more potential use within a VGE, especially the subenvironment “modeling and simulation environment” and its “model standard specification design” as defined by Lin *et al.* (2013). They point out that this requires multidisciplinary perspectives, as this research achieves in incorporating concepts from computer graphics and architectural design. With this history comes well established standards related to sky modeling adopted by the CIE, allowing researchers to reuse these methods and implement them in heterogeneous models, as suggested by Lin *et al.* (2013).

7 Conclusions

Our results indicate that non-directional rendering, with the illumination source most intense near the sky’s zenith and luminosity having radial symmetry, are effective at revealing primary and secondary landforms within negative relief areas such as the Grand Canyon of Arizona and its tributaries and plateaus. This shading effect is best described as “the less visible sky, the darker.” Results also show that directional rendering, including conventional point source rendering, is effective for displaying major landforms with a three-dimensional appearance. Secondary landforms, however, can appear more distinct through the use of more diffuse sources of directional illumination. Specific examples illustrated in this paper include ridgelines and river channels in the Valley and Ridge province of Pennsylvania and glacial valleys and arêtes on Mount Hood in Oregon.

This methodology differs from other cartographic hill-shading techniques that can also be used to highlight secondary terrain features. Use of additional illumination directions to highlight features such as valleys parallel to the illumination vector is well documented by Imhof (1982), and more recently automated within GIS software (e.g. Jenny, 2001). These methods, however, requires expert cartographic knowledge of how variations in shades of gray of secondary landforms will work in concert with the overall hill-shading effect. Another method uses variations in luminosity based on aspect direction (Kennelly and Kimerling, 2004), but this is only possible for certain color combinations and bases colors on maximizing variations in luminosity. Although all of these methods can effectively highlight secondary landforms, none use a single sky model across the entire terrain.

The computer application of Section 4.4 offers a full palette of sky illumination models, including uniform, clear day, overcast, sharp, and the turbid sky models. The computer application allows a map designer to select from among numerous sky models, to see the shading and shadowing effects of a particular model on a sample terrain, and to select a desired number of sky samples. The application outputs a text file of azimuths and inclina-

tions to be used for hill-shading terrain, as well as the weights to apply to the hill-shaded grids before summing all grids as a final rendering true to the sky model selected.

Such an implementation seems a logical first step in moving terrain rendering towards VGEs grounded in explicitly specified, multidisciplinary standards, where such geo-simulations using visibility analysis can be used to create geo-visualizations of terrain or other three-dimensional displays of spatial data.

References

Agarwal, S., Ramamoorthi, R., Belongie, S., and Wann Jensen, H., 2003, Structured importance sampling of environment maps. *ACM Transactions on Graphics*, 22 (8), 605 – 612.

Albrecht, J., 2005. A new age for geosimulation. *Transactions in GIS* 9 (4): 451 – 454.

Benenson, I and Torrens, P., 2004. *Geosimulation: Automata-based Modeling of Urban Phenomena*. Chichester, John Wiley and Sons.

Brassel, K., 1974. A model for automated hill-shading. *American Cartographer*, 1, 15 – 27.

Brassel, K.E., Little, J. and Peucker, T.K., 1974. Automated relief representation. *Annals of the Association of American Geographers*, 64 (4), 610 – 611 and separate folded map (Map Supplement No. 17).

Buttenfield, B.P., Mackaness, W.A., 1991. Visualization. In: Maguire, D.J., Goodchild, M.F., Rhind, D.W. (Eds.), *Geographic Information Systems. Principles, vol. 1*. Longman Scientific and Technical, Harlow, pp. 427 – 443.

Cabral, B., Max, N., and Springmeyer, R., 1987, Bidirectional reflectance functions from surface bump maps. *Computer Graphics (SIGGRAPH)*, 273 – 281.

Chang, K.-T., 2011. *Introduction to geographic information systems*, 6th ed., New York, NY: McGraw-Hill Science/Engineering/Math.

Cook, R. L., Porter, T., and Carpenter, L., 1984. Distributed Ray Tracing, *Computer Graphics*, 18 (3), 137 – 145.

Darula, S. and Kittler, R., 2002. CIE general sky standard defining luminance distributions. In: *Proceedings of eSim*.

Debevec, P., 2005, A median cut algorithm for light probe sampling, *High Dynamic Range Imaging: Acquisition, Display, and Image-Based Lighting*, 430 – 433.

- Dobashi, Y., Kaneda, K., Nakatani, H., Yamashita, H. and Nishita, T., 1995. A Quick Rendering Method Using Basis Functions for Interactive Lighting Design. *Computer Graphics Forum*, 14, 229 – 240.
- Dozier, J., Bruno, J., and Downey, P., 1981. A faster solution to the horizon problem, *Computers & Geosciences*, 7 (2), 145 – 151.
- Dubayah, R., and Rich, P., 1995. Topographic solar radiation models for GIS. *International Journal of Geographical Information Systems*, 9, 405 – 419.
- Fabrikant, S. I., Montello, D. R. , and Mark, D. M., 2010. The natural landscape metaphor in information visualization: The role of commonsense geomorphology. *Journal of the American Society for Information Science and Technology*, 61 (2): 253 – 70.
- Fu., P., and Rich, P., 1999. Design and implementation of the Solar Analyst: An ArcView extension for modeling solar radiation at landscape scales. In: *19th Annual ESRI User Conference*.
- Fu., P. and Rich, P., 2002. A geometric solar radiation model with applications in agriculture and forestry. *Computers and Electronics in Agriculture*, 37: 25 – 35.
- Gibson, K. S. and Tyndall, E. P. T., 1923. The visibility of radiant energy. *U.S. National Bureau of Standards Science Papers*, 19, 131 – 191, paper 475.
- Gillette, G., Pierpoint, W. and Treado, S., 1984. A general daylight illuminance model for daylight availability. *Journal of Illuminating Engineering Society*, July, 330 – 340.
- Greene, N., 1986. Environment mapping and other applications of world projections. *IEEE Computer Graphics and Applications*, 6 (11), 21 – 29.
- Goral, C., Torrance, K., Greenberg, D., and Battaile, B., 1984. Modeling the interaction of light between diffuse surfaces, In Proceedings of the ACM Conference on Computer Graphics, 213 – 222.
- Haber, J., Magnor, M. and Seidel, H.-P., 2005. Physically based simulation of twilight phenomena. *ACM Transactions on Graphics*, 24 (4), 1353 – 1373.
- Halton, J. H., 1970. A retrospective and prospective survey of the Monte Carlo method. *SIAM Review*, 12 (1), 1 – 63.
- Heidrich, W., Daubert, K., Kautz, J., and Seidel, H.-P., 2000. Illuminating micro geometry based on precomputed visibility. *Computer Graphics (SIGGRAPH)*, 455 – 464.
- Heidrich, W. and Seidel, H-P., 1998. View-Independent Environment Maps. In *Eurographics/SIGGRAPH Workshop on Graphics Hardware*, 39 – 45.
- Hobbs, F., 1999. An investigation of RGB multi – band shading for relief visualisation. *The*

International Journal of Applied Earth Observation and Geoinformation, 1 (3–4), 181 – 186.

Hochbaum, D. and D. Shmoys, D., 1985. A best possible heuristic for the k-center problem. *Mathematics of Operations Research*, 10 (2), 180 – 184.

Hopkinson R. G., Petherbridge P. and Longmore J., 1966. *Daylighting*. London: Heinemann.

Igawa, N., Nakamura, H., Matsuzawa, T., Koga, Y., Goto, K. and Kojo, S., 1997. Sky luminance distribution between two CIE standard skies. *Proceedings Lux Pacifica*, E7-E18.

Illuminating Engineering Society of North America, 1993. *Lighting Handbook*. (M.S. Rea, Editor) New York, NY: IESNA.

Imhof, E., 1982. *Cartographic relief presentation*. New York, NY: Walter de Gruyter.

International Commission on Illumination (CIE). Natural daylight. Official Recommendation. 1955. *CIE Proceedings*, Volume 2. Secretariat Committee 3.2, Zurich, 2 – 4.

International Commission on Illumination (CIE). ISO 15469:2004(E) / CIE S 011/E:2003 *Spatial distribution of daylight - CIE standard general sky*, second edition, (February 2004)

Iones, A., Krupkin, A., Sbert, M., and Zhukov, S., 2003. Fast, realistic lighting for video games. *IEEE Computer Graphics and Applications*, 23 (3), 54 – 64.

Iqbal, M., 1983. *An Introduction to Solar Radiation*, Academic Press.

ISO 15469/CIE S003, 1996. *Spatial distribution of daylight - CIE standard overcast sky and clear sky*.

Jenny, B., 2001. An interactive approach to analytical relief shading. *Cartographica*, 38 (1&2), 67 – 75.

Kajiya, J. T., 1986. The rendering equation. *Computer Graphics (SIGGRAPH)*, 20, 143 – 150.

Keller, A., 1997. Instant Radiosity, In Proceedings of the ACM Conference on Computer Graphics, 49 – 56.

Kennelly, P. 2002. Hillshading with oriented halftones. *Cartographic Perspectives*, 43, 24 – 41.

Kennelly, P. and Kimerling, A.J., 2004. Hillshading of terrain using layer tints with aspect-variant luminosity. *Cartography and Geographic Information Science*, 31 (2), 67 – 77.

Kennelly, P., and Stewart, J., 2006. A uniform sky model to enhance shading of terrain and

urban elevation models. *Cartography and Geographic Information Science*, 33 (1): 21 – 36.

Kimball, H.H. and Hand, I.F., 1922. Daylight illumination on horizontal, vertical and sloping surfaces. *Monthly Weather Review*, 50 (12), 615 – 628.

Kimerling, A. J., Muehrcke, J.O. Buckley, A.R. and Muehrcke, P.C. (2010). *Map Use: Reading and Analysis*, 6th ed., Esri Press Academic, Redlands, CA.

Kittler, R., 1967. Standardisation of the outdoor conditions for the calculation of the Daylight Factor with clear skies. In: *Proceedings, Conference Sunlight in Buildings*, Rotterdam: Bouwcentrum, 273 – 286.

Kittler R., Perez R. and Darula S., 1998. A set of standard skies characterizing daylight conditions for computer and energy conscious design. US SK 92 052 Final Report, ICA SAS Bratislava: Polygrafia Bratislava.

Kollig, T., and Keller, A., 2003. Efficient illumination by high dynamic range images. In *Eurographics Workshop on Rendering*, 45 – 51.

Lin, H., Chen, M., and Lu, G., 2013. Virtual geographic environment: A workspace for Computer-Aided Geographic Experiments. *Annals of the Association of American Geographers*, 103 (3): 465 – 482.

MacEachren, A. M., Edsall, R., Haug, D., Otto, G., Masters, R., Fuhrmann, S., and Qian, L. J., 1999. Virtual environments for geographic visualization: Potential and challenges. <http://www.geovista.psu.edu/publications/NPIVM99/ammNPIVM.pdf> (last accessed 30 April 2013).

Maidment, D., 1993. GIS and hydrological modeling. In M. Goodchild, B. Parks, and L. Seyaert (Eds.) *Environmental Modeling with GIS*, 147 – 67. New York: Oxford University Press.

Max, N., 1988. Horizon mapping: shadows for bump-mapped surfaces, *The Visual Computer*, 4 (2), 109 – 117.

Miller, G., 1994. Efficient algorithms for local and global accessibility. *Computer Graphics (SIGGRAPH)*, 319 – 326.

Miller, G. and Hoffman, R., 1984. Illumination and Reflection Maps: Simulated Objects in Simulated and Real Environments. In *SIGGRAPH 1984 Advanced Computer Graphics Animation seminar notes*.

Moellering, H., 2000. The scope and conceptual content of Analytical Cartography. *Cartography and Geographic Information Science*, 27 (3), 205 – 223.

Moellering, H., 2012. Perspectives on 3-D visualization of spatial geodata and future

prospects. In: *True 3-D in Cartography: Autostereoscopic and Solid Visualisation of Geo-data* [Lecture Notes in Geoinformation and Cartography] (Manfred Buchroithner, Editor) Berlin and Heidelberg: Springer Verlag, 1 – 19.

Moon, P., and Spencer, D., 1942, Illumination from a non-uniform sky. *Illumination Engineering*, 37 (10), 707 – 726.

Moore, F., 1985. *Concepts and Practices of Architectural Daylighting*. New York, NY: Van Nostrand Reinhold.

Na, H-S, Lee, C-N and Cheong, O., 2002. Voronoi diagrams on the sphere. *Computational Geometry: Theory and Applications*, 23 (2), 183 – 194.

Nakamura, H., Oki, M. and Hayashi, Y., 1985. Luminance distribution of intermediate sky . *Journal of Light and Visual Environment*, 9 (1), 6 – 13.

Nimeroff, J., Simoncelli, E., and Dorsey, J., 1994. Efficient Re-rendering of Natural Environments, *Eurographics Workshop on Rendering*, 359 – 373.

Nishita, T., and Nakamae, E., 1974. An algorithm for half-toned representation of three-dimensional objects. *Info. Proc. Japan*, 14, 93 – 99.

O’Callaghan, J. F., and Mark, D. M., 1984. The extraction of drainage networks from digital elevation data: Computer Vision, Graphics and Image Processing, Vol. 28, pp. 323-344.

O’Sullivan, D. and Turner, A., 2001. Visibility graphs and landscape visibility analysis. *International Journal of Geographic Information Science*, 15 (3): 221 – 237.

Perez, R., Seals, R., and Michalsky, J., 1993. All-weather model for sky luminance distribution - preliminary configuration and validation. *Solar Energy*, 50 (3), 235 – 245.

Perraudeau, M., 1988. Luminance models. In: *National Lighting Conference*, Cambridge: NLC, 291 – 292.

Peucker, T.K., Tichenor, M. and Rase, W.D., 1974. The computer version of three relief representations. In: *Display and Analysis of Spatial Data* (J.C. Davis and M. McCullagh, Editors). New York, NY: John Wiley & Sons, 187 – 197.

Preetham, A.J., Shirley, P., and Smits, B., 1999. A practical analytic model for daylight. *Computer Graphics (SIGGRAPH)*, 91 – 100.

Ramamoorthi, R., and Hanrahan, P., 2001. An Efficient Representation for Irradiance Environment Maps, In Proceedings of the ACM Conference on Computer Graphics, 497 – 500.

Robbins, C.L. 1985. *Daylighting: Design and Analysis*. New York, NY: Van Nostrand

Reinhold.

Robinson, A. H., Morrison, J. L., Muehrcke, P. C., Kimerling, A. J. and Guptill, S. C., 1995. *Elements of Cartography*, 6th ed., New York, NY: John Wiley & Sons.

Sloan, P-P, Kautz, J., Snyder, J., 2002. Precomputed Radiance Transfer for Real-time Rendering in Dynamic, Low-frequency Lighting Environments, *ACM Transactions on Graphics*, 21 (3), 527 – 536.

Slocum, T. A., McMaster, R. B., Kessler, F. C. and Howard, H. H., 2008. *Thematic cartography and geographic visualization*, 3rd ed., Upper Saddle River, NJ: Pearson Prentice Hall, Inc.

Sloup, J., 2002. A survey of the modelling and rendering of the Earth's atmosphere. In: *Proceedings of SCCG*, 2002.

Spitz, S., and Requicha, A., 2000. Accessibility analysis using computer graphics hardware. *IEEE Transactions on Visualization and Computer Graphics*, 6 (3), 208 – 219.

Steyaert, L. and Goodchild, M., 1994. Integrating geographic information systems and environmental simulation models: a status review. In W. Michener, J. Brunt, and S. Stafford eds., *Environmental Information Management and Analysis: Ecosystem to Global Scales* (Bristol, PA: Taylor & Francis), 333 – 356.

Stewart, J. 1998, Fast horizon computation at all points of a terrain with visibility and shading applications. *IEEE Transactions on Visualization and Computer Graphics*, 4 (1), 82 – 93.

Turner, A., Doxa, M., O'Sullivan, D., and Penn, A., 2001. From isovists to visibility graphs: a methodology for the analysis of architectural space. *Environment and Planning B: Planning and Design*, 28: 103 – 121.

Wang, J., Robinson G., and White, K., 2000. Generating Viewsheds without using Sightlines. *Photogrammetric engineering and remote sensing*, 66 (1), 87 – 90.

Warn, D. R., 1983. Lighting controls for synthetic images. *Computer Graphics (SIGGRAPH)*, 17 (3), 13 – 21.

Wiechel, H., 1878. Theorie und darstellung der beluchtung von nicht gesetzmassig gebildeten flachen mit rucksicht auf die bergzeichnung. *Civilingenieur*, 24, 335 – 364.

Wood, J., Kirschenbauer, S., Dllner, J., Lopes, A., and Bodum, L., 2005. Using 3D in Visualization. In *Exploring Geovisualizaiton* (J. Dykes, A MacEachren, and M-J Kraak (Eds.). New York: Oxford: Pergamon.

Yoeli, P., 1959. Relief shading. *Surveying and Mapping*, 19 (2), 229 – 232.

- Yoeli, P., 1965. Analytical hill shading. *Surveying and Mapping*, 25 (4), 573 – 579.
- Yoeli, P., 1966. Analytical hill shading and density. *Surveying and Mapping*, 26 (2), 253 – 259.
- Yoeli, P., 1967. The mechanisation of analytical hill shading. *Cartographic Journal*, 4, 82 – 88.
- Yuan, M., 1999. Use of a three domain representation to enhance GIS support for complex spatiotemporal queries. *Transactions in GIS* 3: 137 – 59.
- Zhukov, S., Inoes, A., and Kronin, G., 1998. An ambient light illumination model. *Eurographics Workshop on Rendering*, 45 – 56.
- Zotti G., Wilkie A. and Purgathofer W., 2007. A critical review of the Preetham skylight model. In: *WSCG 2007 Short Communications Proceedings I*, 23 – 30.

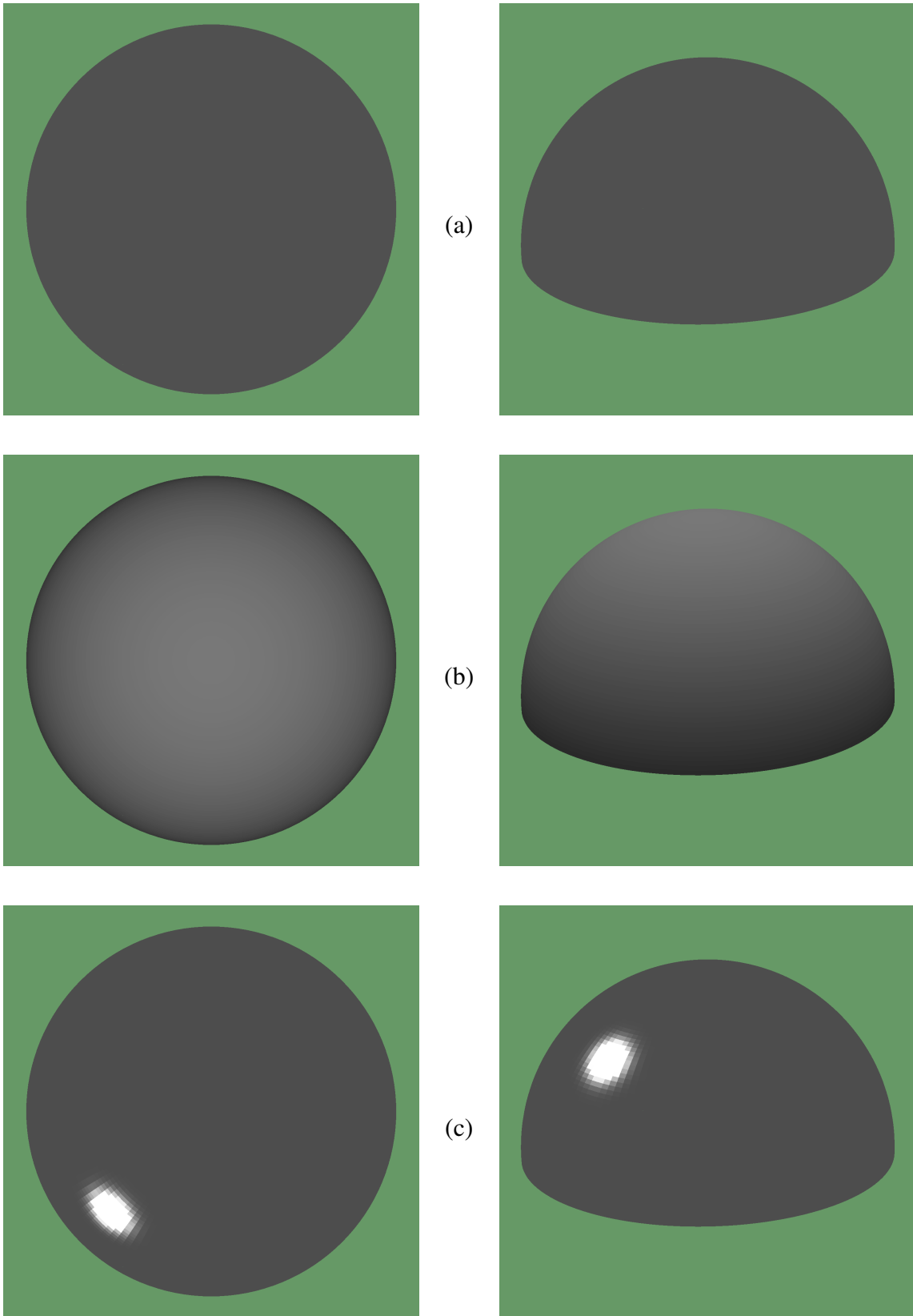


Figure 1: Continued on next page.

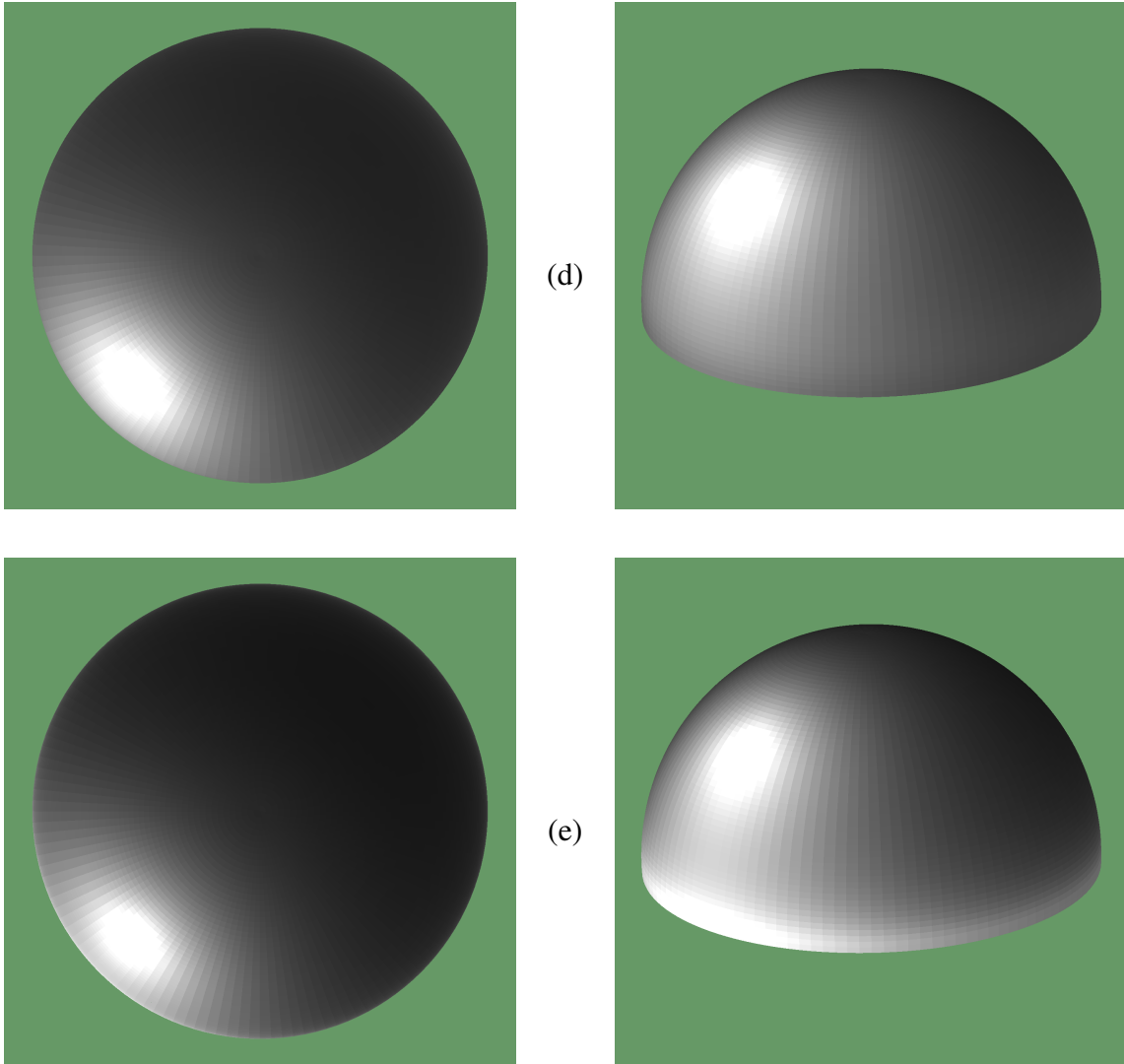


Figure 1: The radiance for (a) uniform, (b) overcast, (c) sharp, (d) clear, and (e) turbid skies. In the left column, the center of the circle corresponds to an inclination of 90 degrees and the circumference an inclination of 0 degrees. In the right column, the radiance is shown on the side of a hemisphere, where each point represents one direction from the sky.

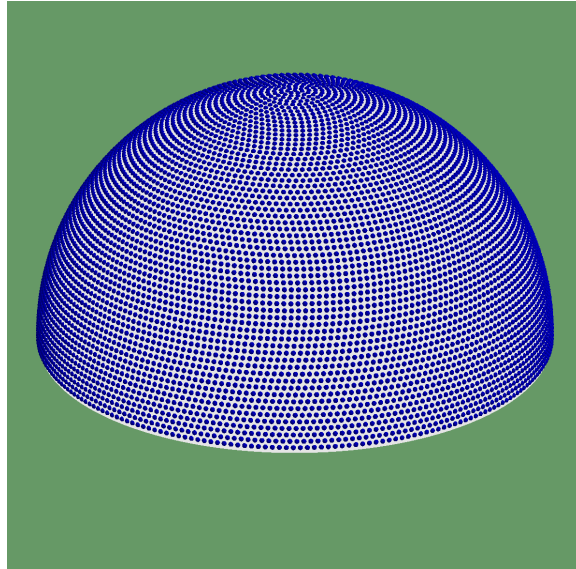
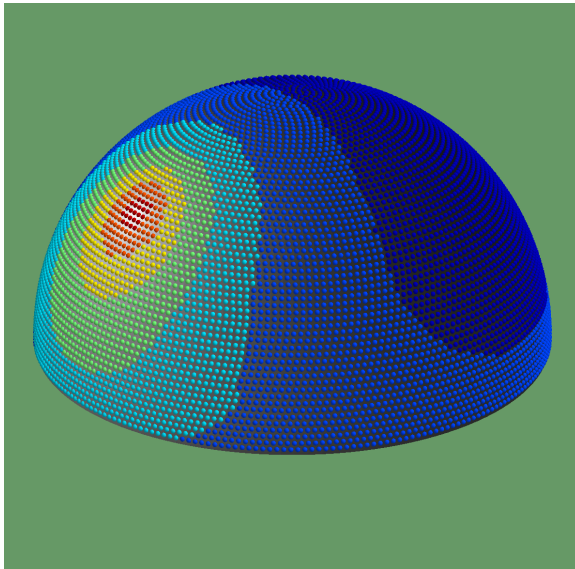
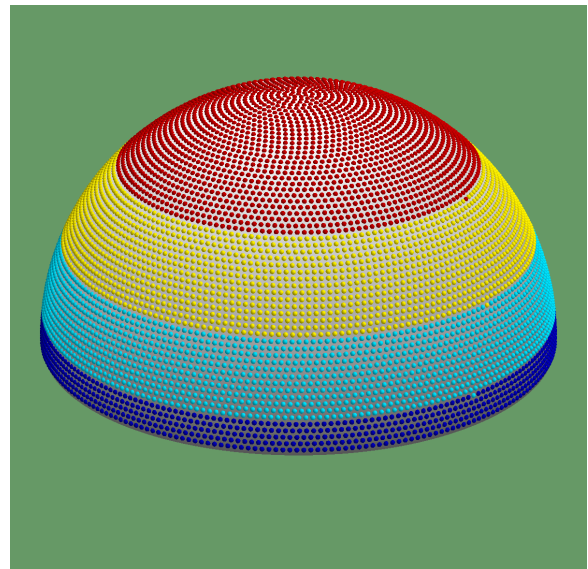


Figure 2: The initial sampling of the sky hemisphere using 9956 sample directions, each of which represents approximately the same solid angle of the sky.

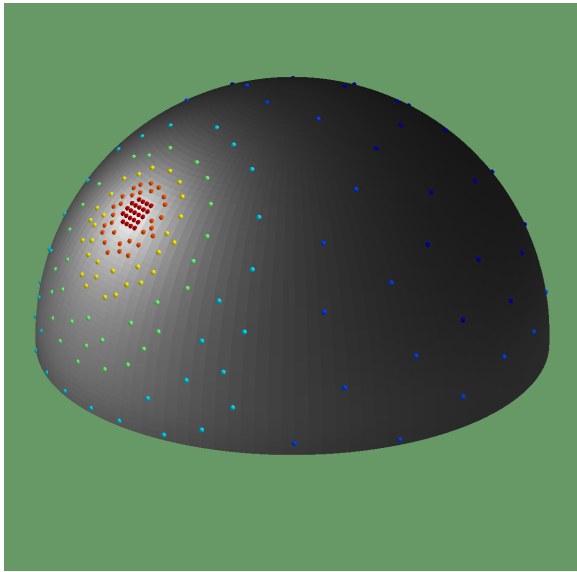


strata in the clear sky

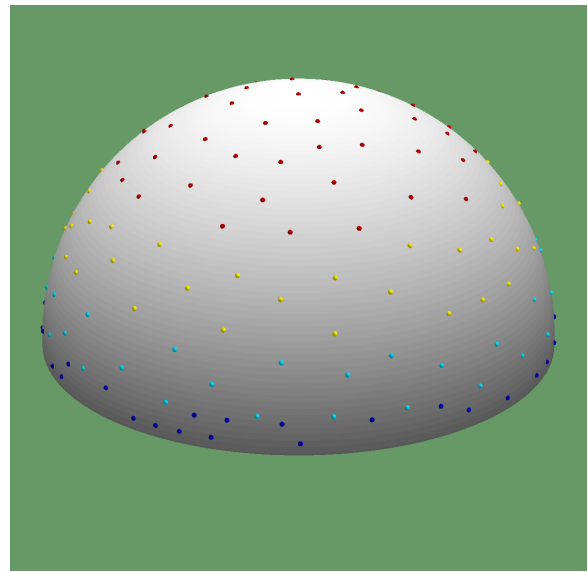


strata in the overcast sky

Figure 3: Seven strata of the sky; only four strata are present in the overcast sky because there is less variance in illumination. Each stratum contains a range of radiances equal to one standard deviation of all the radiances

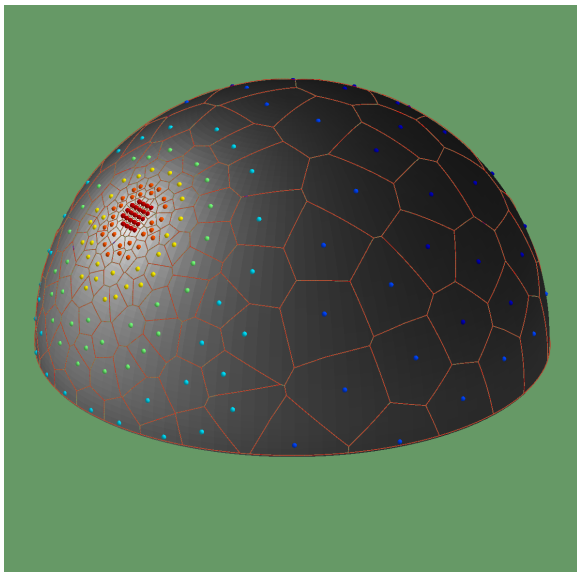


samples in the clear sky

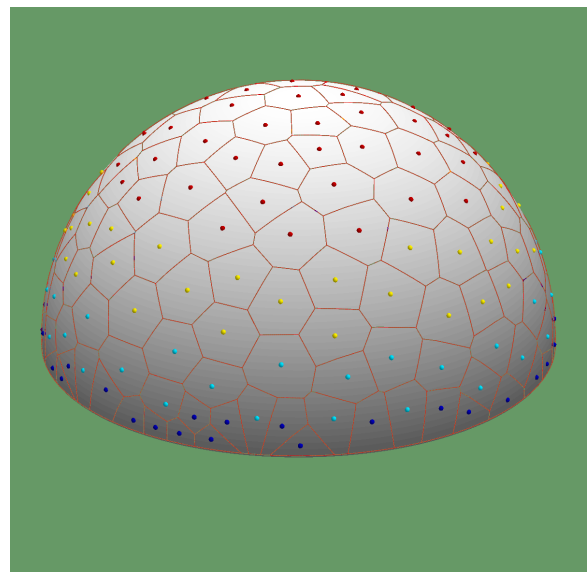


samples in the overcast sky

Figure 4: The subset of sample directions chosen within each stratum. Each stratum has an even distribution of 29 or 30 samples. In the general sky, darker strata have less dense samples, each of which is responsible for a larger solid angle.

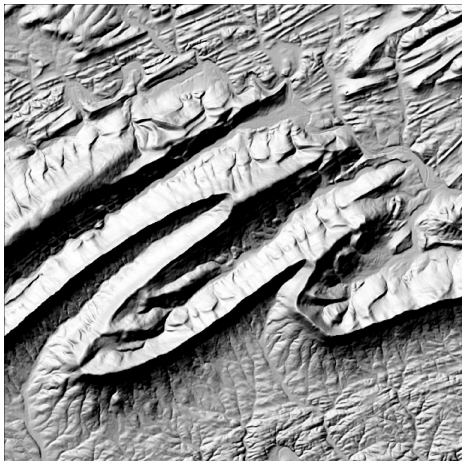


regions in the clear sky

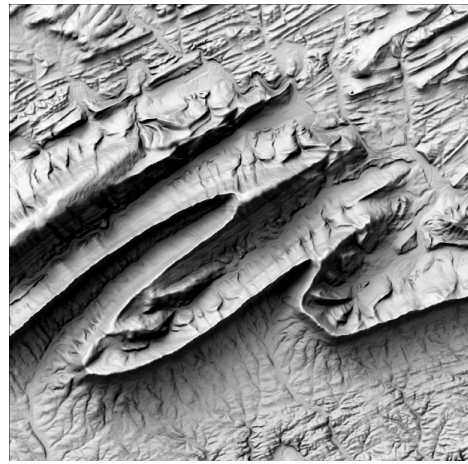


regions in the overcast sky

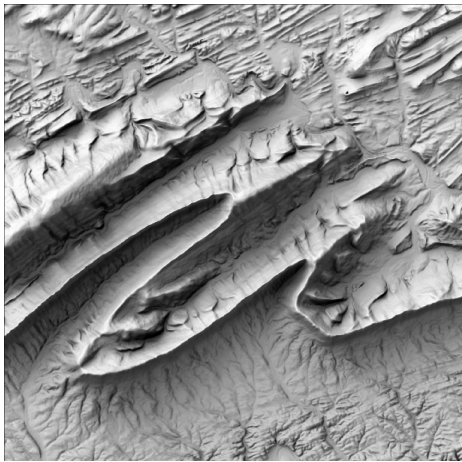
Figure 5: The Voronoi cells around each sample point. The weight of a sample point is proportional to the solid angle subtended by its Voronoi cell. In brighter areas there is a denser sampling, but each sample has lower weight.



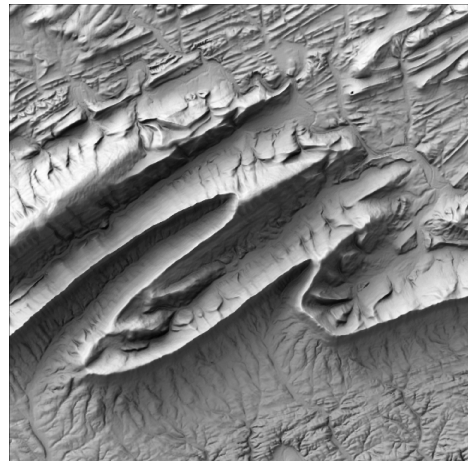
(a) Point Source



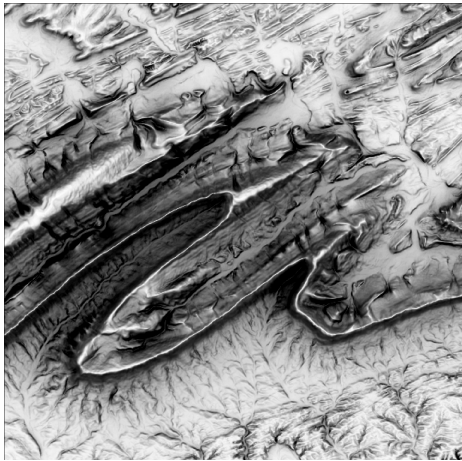
(b) Sharp



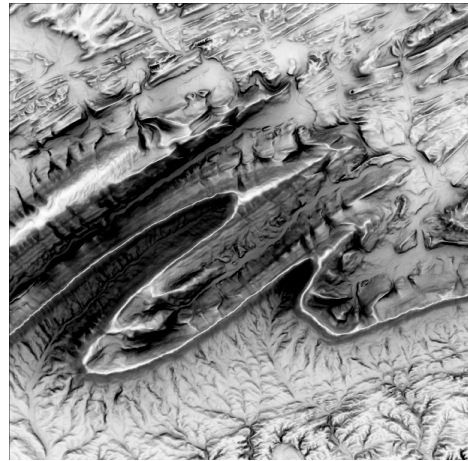
(c) Clear Day



(d) Turbid Sky

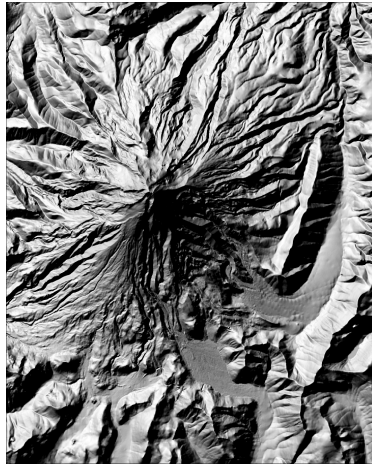


(e) Overcast Sky

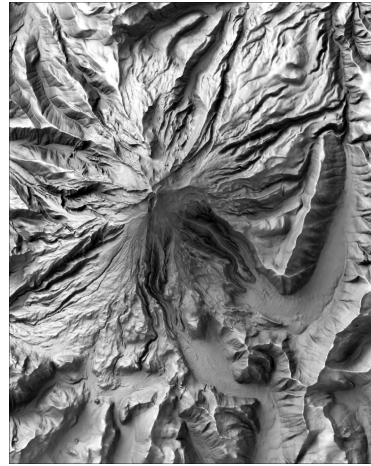


(f) Uniform

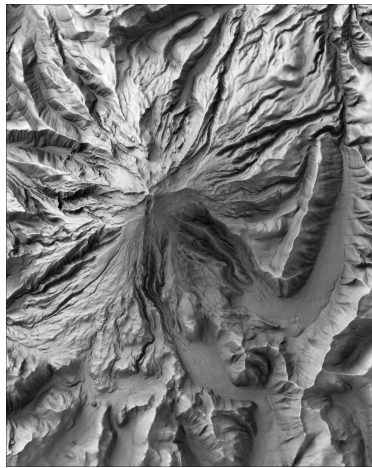
Figure 6: Renderings of a portion of the Valley and Ridge province, Pennsylvania using various sky models.



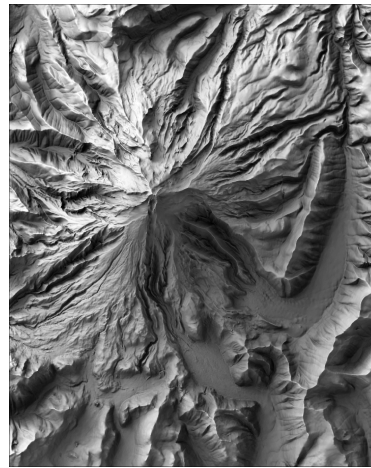
(a) Point Source



(b) Sharp



(c) Clear Day



(d) Turbid Sky



(e) Overcast Sky



(f) Uniform

Figure 7: Renderings of Mt. Hood, Oregon using various sky models.



(a) Point Source



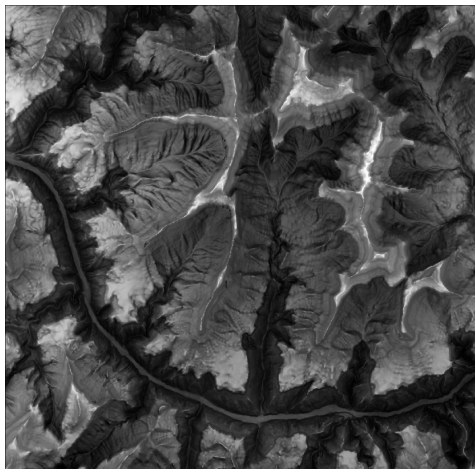
(b) Sharp



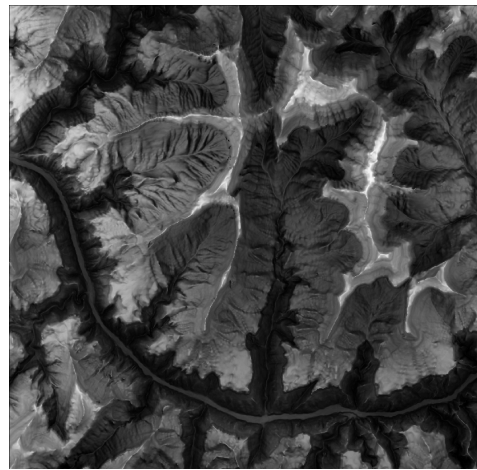
(c) Clear Day



(d) Turbid Sky



(e) Overcast Sky



(f) Uniform

Figure 8: Renderings of a portion of the Grand Canyon, Arizona using various sky models.